Extended Abstracts of the 2016 International Conference on Solid State Devices and Materials, Tsukuba, 2016, pp181-182

D-1-02

Formation and utilization of composition engineered transition regions across 2D metal-semiconductor atomic layer junctions

Byungjin Cho[1], Yonghoon Kim[1], Myung Gwan Hahm[2] and Pulickel M. Ajayan[3]

[1]Department of Advanced Functional Thin Films, Korea Institute of Materials Science, 797 Changwondaero, Sungsan-gu, Changwon, Gyeongnam 51508, Republic of Korea; Email: bjcho@kims.re.kr
[2]Depaertement of Materials Science and Engineering, Inha University, 100 Inharo, Nam-Gu, Incheon 22212, Republic of Korea
[3]Department of Materials Science and Nano Engineering, Rice University, 6100 Main Street, Houston, Texas 77005, USA

Abstract

We demonstrate that interfacial alloying can be achieved between semiconducting WSe_2 transition metal dichalcogenide (TMD) channels and metallic $NbSe_2$ TMD contact layers, forming metallic $Nb_xW_{1-x}Se_2$ interfacial layers that aid in forming excellent electrical contact between the semiconducting and metallic TMD regions. This interfacial transition $Nb_xW_{1-x}Se_2$ structure considerably lowers the potential barrier height of the junction between 2D semiconductor-metal regions leading to significantly improved performance of the WSe_2 based transistor device. The creation of such composition engineered transition regions across 2D junctions between dissimilar TMD domains could be most important in the design and fabrication of 2D atomic layer devices.

1. Introduction

Among 2D atomic layer building blocks such as graphene, hexagonal boron nitride, and TMDs, atomically thin TMDs are excellent 2D semiconductors owing to the presence of a finite bandgap and various other interesting electronic properties.[1] Combining compositional different atomic layers in to van der Waals (vdW) heterostructures have gained interest due to the possibility of generating a large number of electronically variant systems.[2,3] Interfacial contact resistance is among the critical issues to be addressed owing to the formation of a Schottky barrier.[4] Here, we demonstrate a 2D semiconductor-metal system with low interfacial contact resistance in TMDs-based electronic devices by creating a transition region with mixed composition between the 2D semiconductor and metallic regions of the device system.

2. Results

In this proposed approach, we first designed a simple bottom-gate field effect transistor (FET) using WSe_2 channel and $NbSe_2$ contact. Figures 1a and 1b present the optical image and schematic drawing of the designed FET. The semiconducting WSe_2 (the bottom layer) and the patterned $NbSe_2$ (the top layer) electrical contacts were synthesized on a heavily doped silicon oxide wafer using a single-step chemical vapor deposition (CVD) process. Tungsten trioxide (WO_3) and niobium pentoxide (Nb_2O_5) thin films were

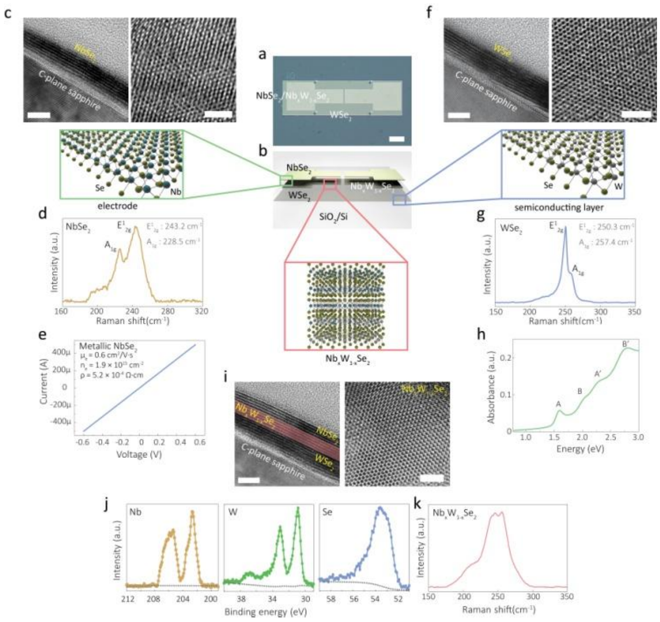

Fig. 1. Synthesis of semiconducting WSe_2 and metallic $NbSe_2$ with transition $Nb_xW_{1-x}Se_2$ layer. (a) Optical image of the WSe_2-based bottom gate field effect transistor with $NbSe_2$ electrode. The scale bar is 10 μm. (b) Schematic of the transistor and crystal structure of the metallic $NbSe_2$ (the green box), the semiconducting WSe_2 (the blue box), and the transition $Nb_xW_{1-x}Se_2$ layer. (c) Cross-sectional and top views of high-resolution transmission electron microscopy (HR-TEM) images of the as-grown $NbSe_2$ film. The scale bars are 5 nm each. (d) Raman spectrum recorded from the as-synthesized $NbSe_2$ film. (e) Hall measurement result, showing that the as-synthesized $NbSe_2$ film has metallic characteristics. (f) Cross-sectional and top views of HR-TEM images of the as-grown $NbSe_2$ film. The scale bars are 5 nm each. The cross-sectional images (c and f) show that the as-grown $NbSe_2$ and WSe_2 are multi-layered, while top view images show the crystallinities of $NbSe_2$ and WSe_2. (g) Raman spectrum recorded from the as-synthesized $NbSe_2$ film. Two spectra (d and g) show two major phonon modes: an out-of-plane mode (A_{1g}) and an in-plane mode (E^1_{2g}). (i) Cross-sectional HR-TEM image, showing the transition $Nb_xW_{1-x}Se_2$ layer (red) between $NbSe_2$ and WSe_2 (left), and top view image showing the quasi-hexagonal honeycomb atomic structure. The scale bars are 5 nm each. (j) The XPS spectra show the chemical composition (Nb, W, and Se) of the transition $Nb_xW_{1-x}Se_2$ layer. (k) The Raman spectrum shows the four overlapping vibrational modes of Nb-Se (A_{1g} and E^1_{2g}) and W-Se (E^1_{2g} and A_{1g}).

simultaneously selenized at 1000 °C in the CVD process. Figures 1c and 1f show the high-resolution transmission electron microscopy (HR-TEM) images of cross-sectional and top views of as-synthesized WSe_2 and $NbSe_2$, respectively. Figures 1d and 1g show the Raman spectra recorded from the surfaces of $NbSe_2$ and WSe_2 films, respectively The spectra exhibit two phonon modes: A_{1g} and E^1_{2g} to an in-plane mode).[5] In Figure 1e, the Hall measurement results show that the as-synthesized $NbSe_2$ film has metallic characteristics and the majority carriers are electrons. In Figure 1h, excitonic absorption peaks A and B of the optical absorbance spectrum recorded from the as-synthesized WSe_2 correspond to direct gap transitions at the K point of the Brillouin zone. The most interesting aspect of this work is the formation of a transition interfacial region between semiconducting WSe_2 and metallic $NbSe_2$ during the CVD process. Figure 1i shows the cross-sectional and top views of HR-TEM images acquired from the heterostructure. In Figure 1j, the XPS spectra reveal the chemical composition (Nb, W, and Se) for this transition $Nb_xW_{1-x}Se_2$ layer. Shown in Figure 1k, the Raman spectrum exhibits four overlapping vibrational modes of Nb-Se (A_{1g} and E^1_{2g}) and W-Se (E^1_{2g} and A_{1g}).

We turned our attention to electrical properties of FET devices to compare junction characteristics (typical metal (Pd) -semiconducting WSe_2 (MS), the 2D $NbSe_2$-WSe_2 van der Waals (vdW), and the mixed layer containing $NbSe_2$-$Nb_xW_{1-x}Se_2$-WSe_2 van der Waals (m-vdW) junctions). Figure 2a shows the output I_{DS}-V_{DS} (drain-source current vs. drain voltage) curves for each device. Asymmetrical and nonlinear characteristics of the MS and vdW junctions clearly indicate a Schottky junction, while the m-vdW junction exhibits a relatively symmetry and linear I_{DS}-V_{DS} behavior. The drain currents considerably increased after introducing the metallic $NbSe_2$. The contact resistance of the m-vdW junction was reduced more dramatically compared with that of the MS junction, which was responsible for increasing the probability of charge injection through the transition $Nb_xW_{1-x}Se_2$ atomic layer (Figure 2b). $Nb_xW_{1-x}Se_2$ exhibits the majority of hole carriers, as Nb dopants on WSe_2 shift the Fermi level below the valence band minimum. Such a high concentration of carriers at the interface reduces the effective Schottky barrier height. Also, the transfer characteristics (I_{DS}-V_{BG}) of the m-vdW FET device exhibit larger ON current compared with those of the MS and vdW devices (Figure 2c). Improvement of output characteristics of WSe_2–based FET devices can also be the result of superior contact properties of $NbSe_2$-based electrodes (Figure 2d).

We also evaluated the drain currents at different temperatures to extract barrier heights using the thermionic emission model. From the Arrhenius plot of $\ln(I_{DS}/T^{3/2})$ versus 1000/T at fixed drain voltage of 0.5 V, the measured slopes for the MS, vdW, and m-vdW devices were -7.05, -3.90, and -1.77, respectively, as shown in Figure 2e. The estimated Schottky barrier heights for the MS, vdW, and m-vdW devices, based on the extrapolation curves of the slopes vs. V_{DS}, were 0.81, 0.35, and 0.15 eV (Figure 2f). The m-vdW junction was most effective in lowering the electronic contact barrier height.

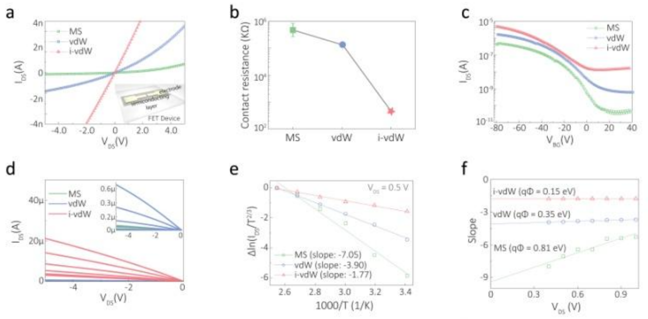

Fig. 2. Junction-dependent electrical properties of the WSe_2-based bottom gate field effect transistor. (a) I_{DS}-V_{DS} (drain current vs. drain voltage) characteristics of metal-semiconducting WSe_2 (MS), $NbSe_2$-WSe_2 van der Waals (vdW), and mixed $NbSe_2$-$Nb_xW_{1-x}Se_2$-WSe_2 van der Waals (m-vdW) junctions. Drain current (I_{DS}) was measured at the drain voltage (V_{DS}) ranging from -5 to 5 V, and back gate voltage (V_{BG}) of 0 V. (b) Comparison of the contact resistances for the MS, vdW, and m-vdW devices. The contact resistances were extracted at the channel lengths of 10 to 50 μm, using the transmission line method. (c) Transfer characteristics (I_{DS}-V_{BG}) of the MS, vdW, and m-vdW junction devices. I_{DS} was measured at the V_{DS} of -5 V on devices with the channel length of 50 μm and width of 100 μm. (d) Output characteristics (I_{DS}-V_{DS} modulated by V_{BG}). V_{BG} from -50 to 0 V (steps of 10 V) was applied for modulating the I_{DS}-V_{DS} curves of the FET devices. (e) Arrhenius plot of $\ln(I_{DS}/T^{3/2})$ against 1000/T, at a fixed drain voltage of 0.5 V, for the MS, vdW, and m-vdW junction devices based on the 2D thermionic emission model. Temperature range was 293 to 393 K. The absolute value of the slope is proportional to the Schottky barrier height. (f) The Schottky barrier heights of the MS, vdW, and m-vdW junction devices. In each case, the Schottky barrier height was calculated from the Y-intercept value on the extrapolation curve of the slope vs.

3. Conclusions

We have shown an effective vapor phase growth strategy for alloyed atomic layers between semiconducting WSe_2 and metallic $NbSe_2$. The presence of a $Nb_xW_{1-x}Se_2$ alloy atomic layer in between the semiconducting WSe_2 and metallic $NbSe_2$ layers considerably reduces the contact resistance, leading to excellent high ON current of WSe_2 FET. The Schottky barrier lowering and tunneling are simultaneously considered for describing the enhanced charge transport throughout such novel mixed 2D atomic layer heterojunctions. The composition engineering of junctions in 2D atomic layer heterostructures promises to create novel 2D electronic devices.

Acknowledgements

This study was supported by the Fundamental Research Program (PNK4580 and PNK4890) of the Korean Institute of Materials Science.

References

[1] Radisavljevic, B., Radenovic, A., Brivio, J., Giacometti, V. & Kis, A. Nat. Nanotechnol. **6,** 147–150 (2011).
[2] Gong, Y. et al. Nat. Mater. **13,** 1135-1142 (2014).
[3] Lee, C.-H. et al. Nat. Nanotechnol. **9,** 676–681 (2014).
[4] Kappera, R. et al. Nat. Mater. **13,** 1128-1134 (2014).
[5] Terrones, H. et al. Sci. Rep. **4,** 4215 (2014).